

SUPPORTING INFORMATION

Effect of Cu(II) on Mn(II) Oxidation by Free Chlorine to Form Mn Oxides at Drinking

Water Conditions

Guiwei Li,^{†,‡,§} Weiyi Pan,[‡] Lili Zhang,[†] Ziqiao Wang,[†] Baoyou Shi^{†,§}

and Daniel E. Giammar^{*,‡}

[†]Key Laboratory of Drinking Water Science and Technology, Research Center for Eco-Environmental Sciences, Chinese Academy of Sciences, Beijing 100085, China

[‡]Department of Energy, Environmental and Chemical Engineering, Washington University in St. Louis, St. Louis, Missouri 63130, United States

[§]University of Chinese Academy of Sciences, Beijing 100049, China

*Corresponding author.

E-mail address: giammar@wustl.edu

Prepared January 11, 2020

This file includes supplementary text and figures:

- 17 pages

- 14 Figures

Table of contents

Sample preparation for SEM and TEM	S3
Figure S1. Species of dissolved Mn(II), free chlorine and solubility of Mn minerals	S4
Figure S2. The calculated concentrations of DIC in equilibrium with atmospheric CO ₂	S5
Figure S3. Mn(II) oxidation in Cu-free system	S5
Figure S4. Cu(II) concentration change in a system without Mn	.S7
Figure S5. Species of dissolved Cu(II) and solubility of Cu minerals	S8
Figure S6. Decrease of dissolved Cu(II) concentration during Mn(II) oxidation	S9
Figure S7. SEM images of MnO _x formed in Cu(II)-containing system	S10
Figure S8. EDS analysis of MnO _x -Cu(II)	S11
Figure S9. TEM images and zeta potential of MnO _x in Cu-free system	S12
Figure S10. Comparison of dissolved Mn(II) defined by 0.22 µm and 10 kDa filters	S13
Figure S11. Zeta potential of MnO _x formed in Cu(II)-containing system	S14
Figure S12. SEM-EDS analysis of Mn formed in CuO-containing system	S15
Figure S13. Temperature effect on Mn(II) oxidation catalyzed by Cu(II) and CuO	S16
Figure S14. Effect of TBA on Mn(II) oxidation with Cu(II) present	S17

TEM (transmission electron microscopy) sample preparation. Transmission electron microscopy (TEM) was used to visualize particle size. During the oxidation of Mn(II), 10 μ L of the MnO_x-containing suspension was placed on a carbon-coated copper grid and then dried at room temperature.

SEM (scanning electron microscope) sample preparation. As the oxidation of Mn(II) could be greatly affected by its initial concentration, a dose of Mn(II) of 100 μ g/L was adopted in all the experiments of this study. This is a typical regulatory level of Mn in finished water as well as a typical concentration of Mn found in drinking water distribution systems. As a result, it could be very challenging to collect particles from water samples for the characterization of Mn(II) oxidation products. However, it was found that after Mn(II) oxidation, there were some fine Mn particles deposited on the surface of stir bars used for water mixing. Particles were collected carefully from the stirrer bar for SEM characterization: the stir bar was first immersed in ethyl alcohol and sonicated to disperse Mn oxides; one drop of the MnO_x-containing alcohol was then placed on a silica wafer, and the alcohol evaporated before the sample was taken to the SEM for characterization.

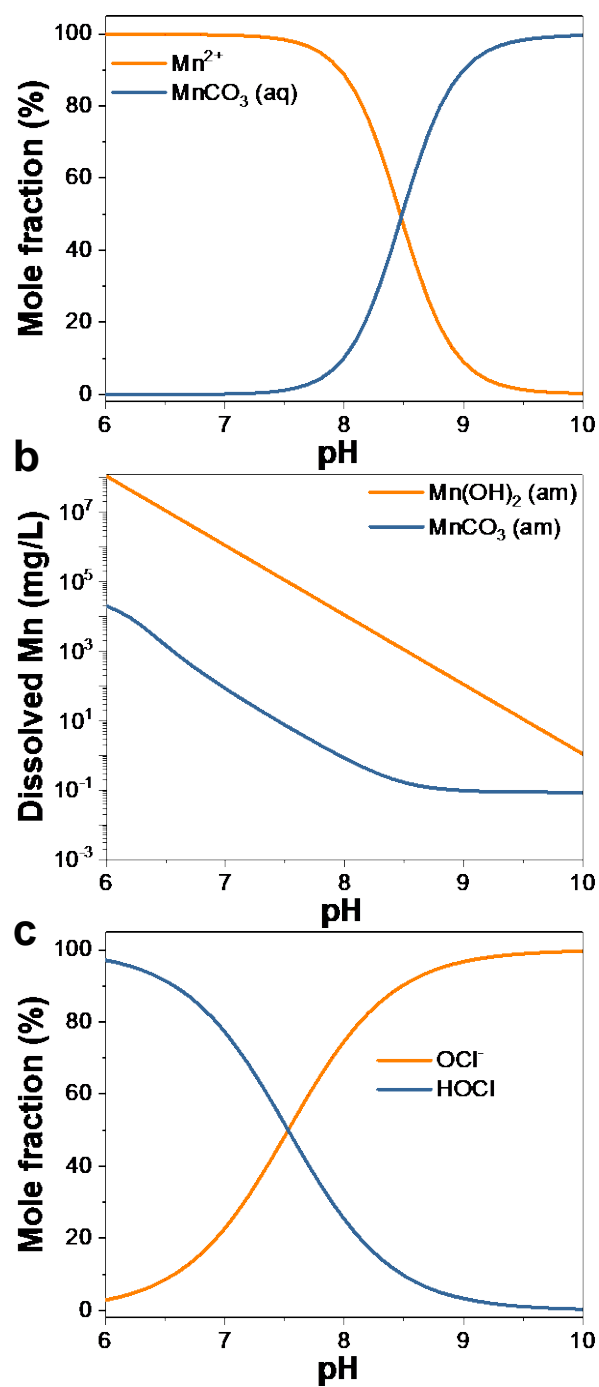


Figure S1. (a) Speciation of dissolved Mn(II) (100 $\mu\text{g/L}$) in an open system with DIC in equilibrium with atmospheric CO_2 at 25 $^\circ\text{C}$. (b) Solubility of MnCO_3 with DIC in equilibrium with atmospheric CO_2 at 25 $^\circ\text{C}$, and the solubility of Mn(OH)_2 without DIC at 25 $^\circ\text{C}$. (c) Speciation of free chlorine ($\text{HOCl} + \text{OCl}^-$) with different pH. Visual MINTEQ 3.1 was used for the calculation.

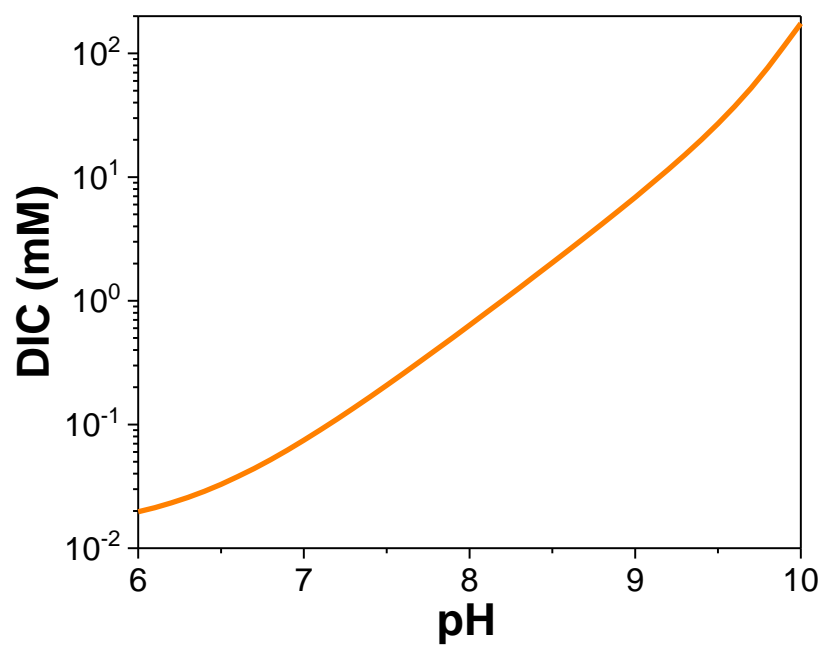


Figure S2. Concentrations of DIC in equilibrium with atmospheric CO₂ calculated by Visual MINTEQ3.1, based on a CO₂ partial pressure of 400 ppm.

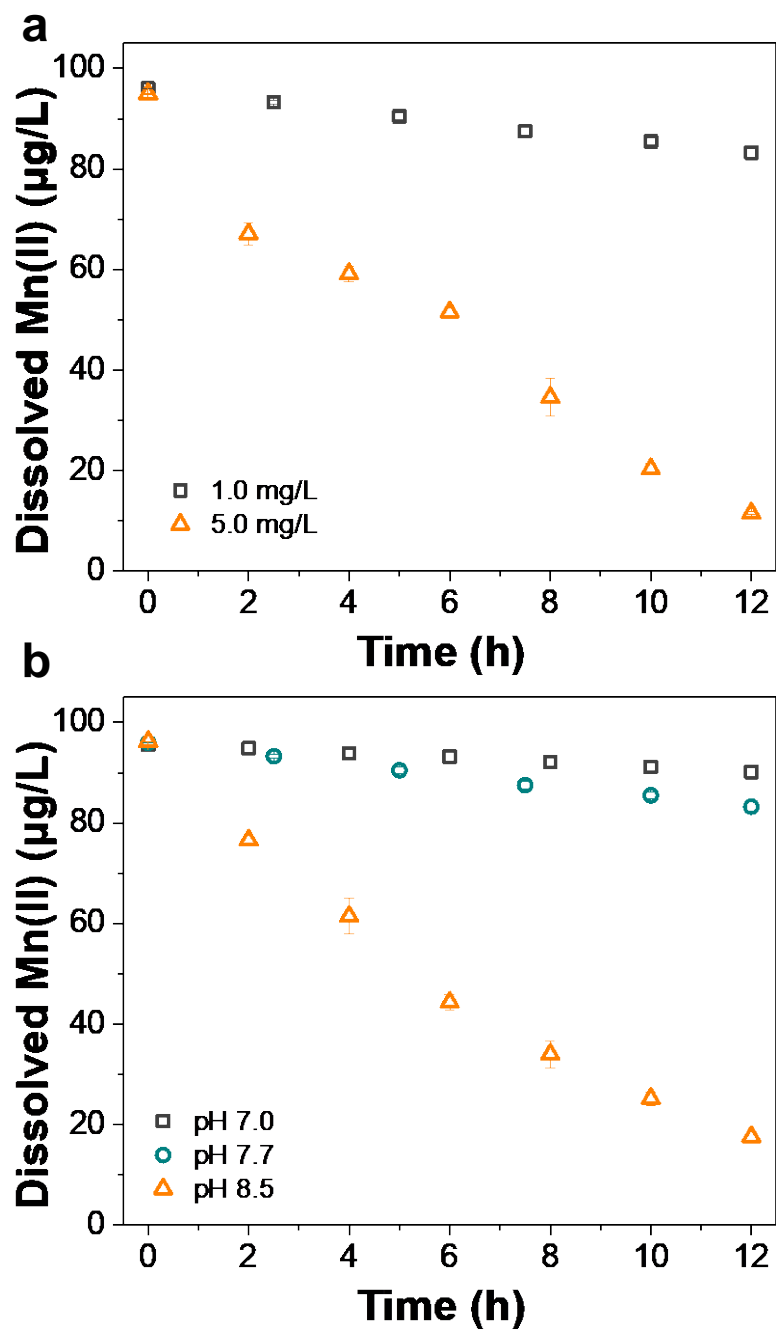


Figure S3. Oxidation of 100 $\mu\text{g/L}$ (1.82 μM) Mn(II) (a) by different concentrations of chlorine at pH 7.7 ± 0.1 and (b) by 1.0 mg/L Cl_2 (14.1 μM) at different pH. Other experimental conditions: NaCl = 1.0 mM, open to air. The error bars are the standard deviations of duplicate experiments.

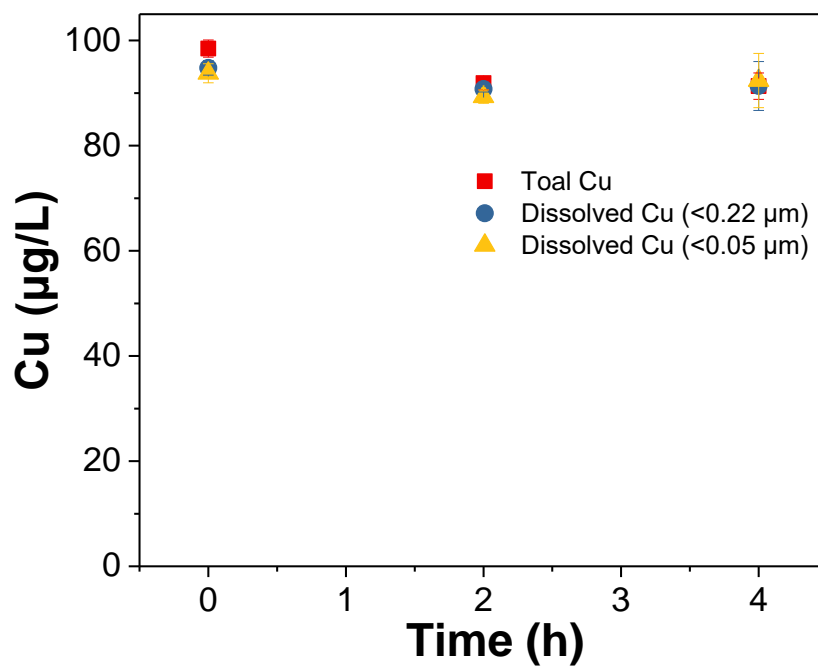


Figure S4. Concentration of dissolved Cu(II) in solutions without Mn(II) or chlorine present. Experimental conditions: NaCl = 1.0 mM, pH = 7.7 ± 0.1 , open to air. The error bars are the standard deviations of duplicate experiments.

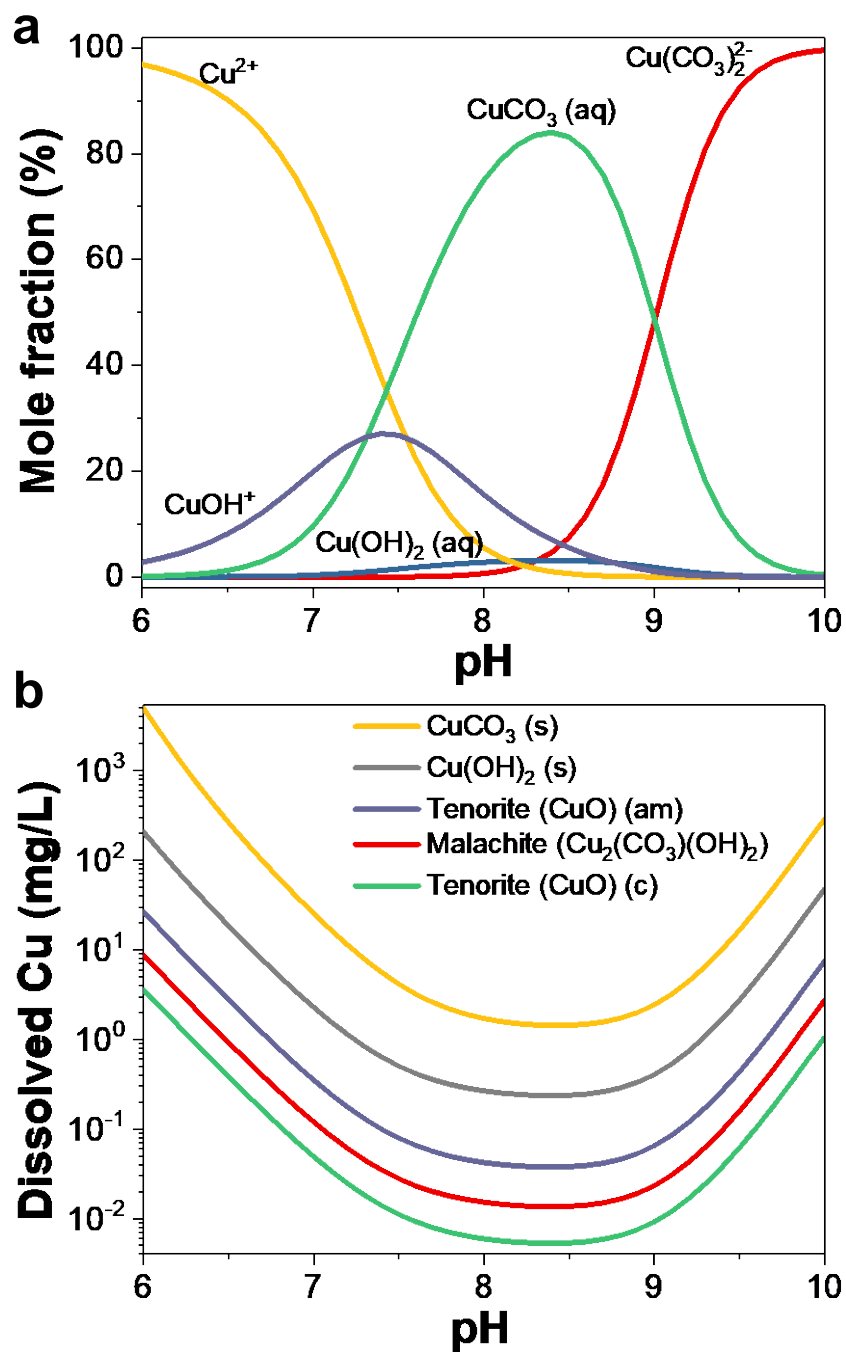


Figure S5. (a) Solubility of Cu(II) minerals and (b) dissolved species of Cu(II) (100 $\mu\text{g/L}$) at pH ranging from 6.0 to 10.0. $T = 25^\circ\text{C}$, $\text{NaCl} = 1.0 \text{ mM}$, DIC in equilibrium with atmosphere at pH ranging from 6.0 to 9.0. The calculations were performed using Visual MINTEQ 3.1.

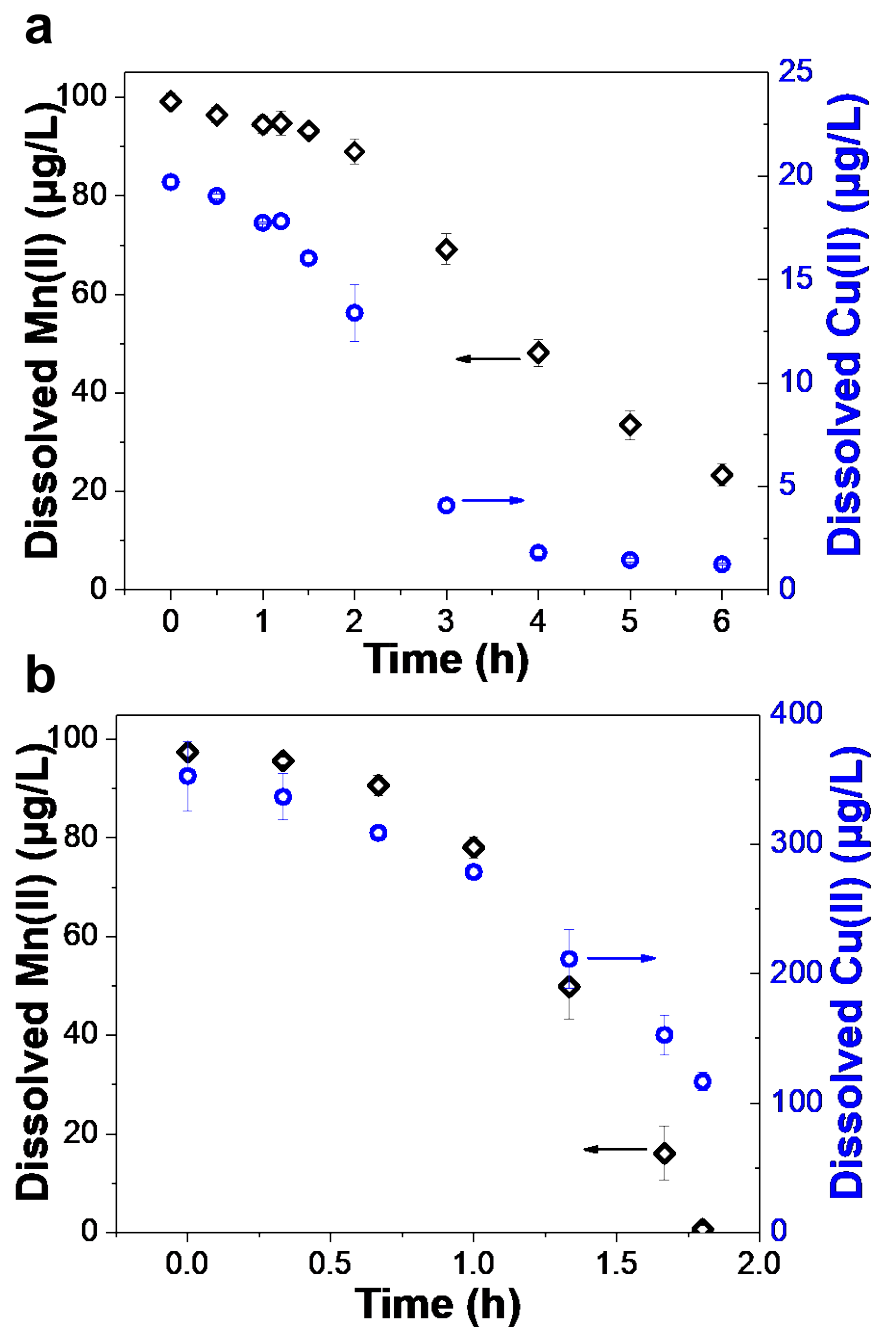


Figure S6. Decrease of dissolved Cu(II) and Mn(II) concentrations during the oxidation of Mn(II) by free chlorine: (a) initial Cu(II) dose = 20 $\mu\text{g/L}$, (b) initial Cu(II) dose = 400 $\mu\text{g/L}$. Experimental conditions: NaCl = 1.0 mM, Cl_2 = 1.0 mg/L, pH = 7.7 ± 0.1 , open to air. The error bars are the standard deviations of duplicate experiments.

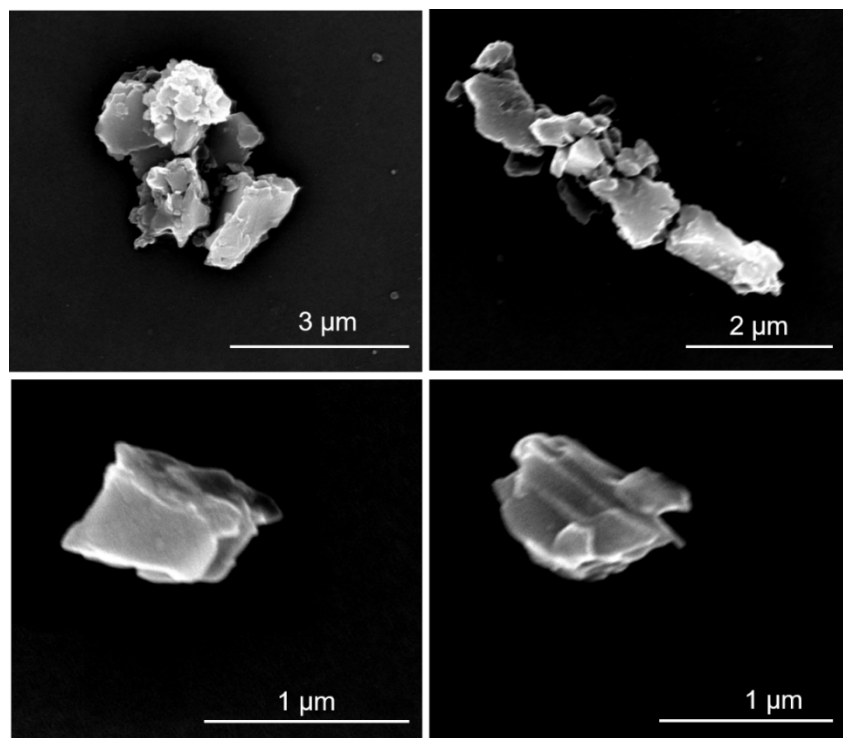


Figure S7. SEM images of MnO_x particles formed from the Mn(II) oxidation in the presence of dissolved Cu(II). Experimental conditions: NaCl = 1.0 mM, Mn(II) = 100 μg/L, Cu(II) (added in the form of CuSO₄) = 100 μg/L, pH = 7.7 ± 0.1, open to air; reaction proceeded for 4 hours. Four images were collected to make them more representative and they were all for the same batch of solid sample.

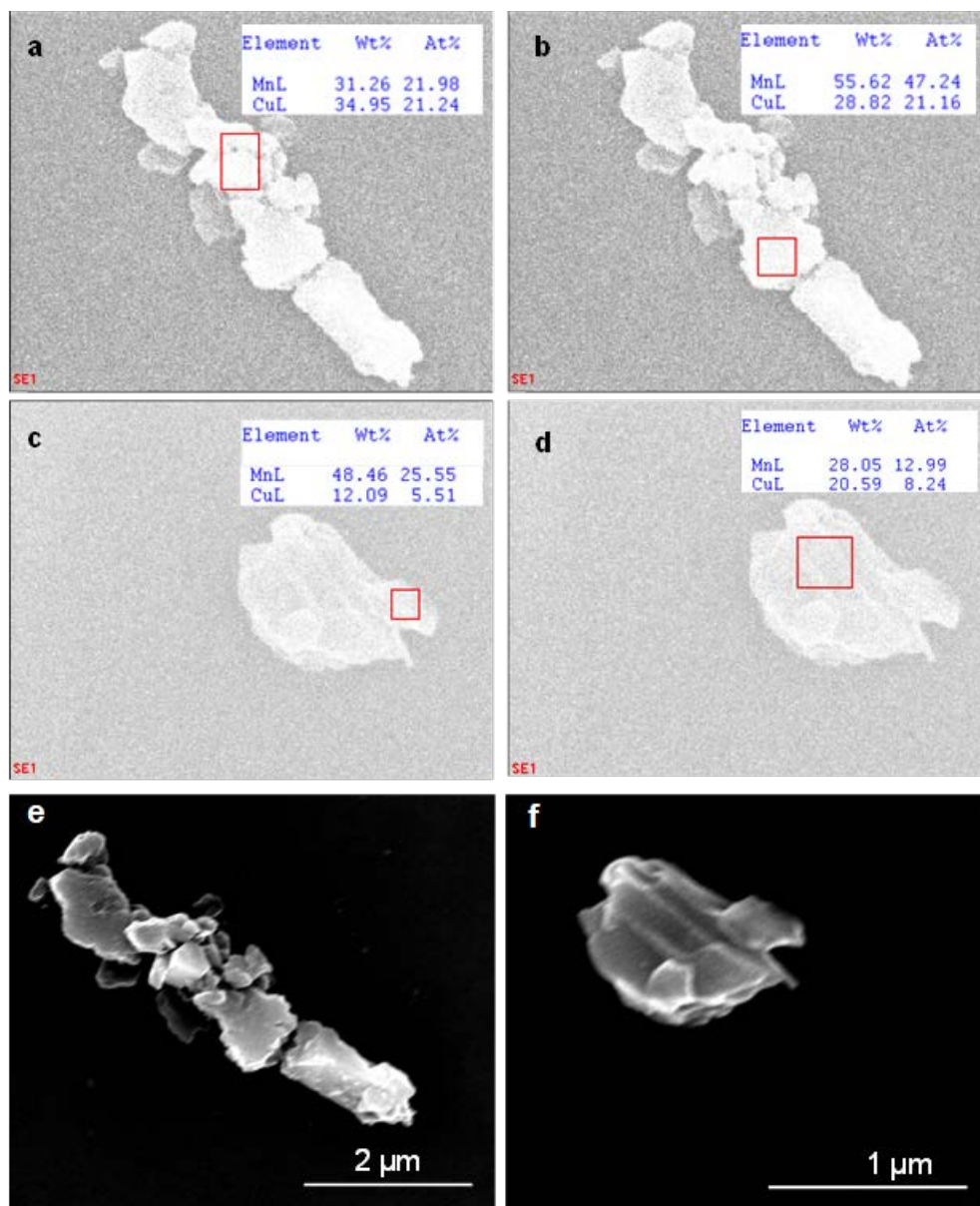


Figure S8. (a) and (b), Mn and Cu contents detected by EDS at two locations on the surface of MnO_x-Cu(II) particle_1; (c) and (d), Mn and Cu contents detected by EDS at two locations on the surface of MnO_x-Cu(II) particle_2. (e) and (f) are for clearer viewing of MnO_x particulates.

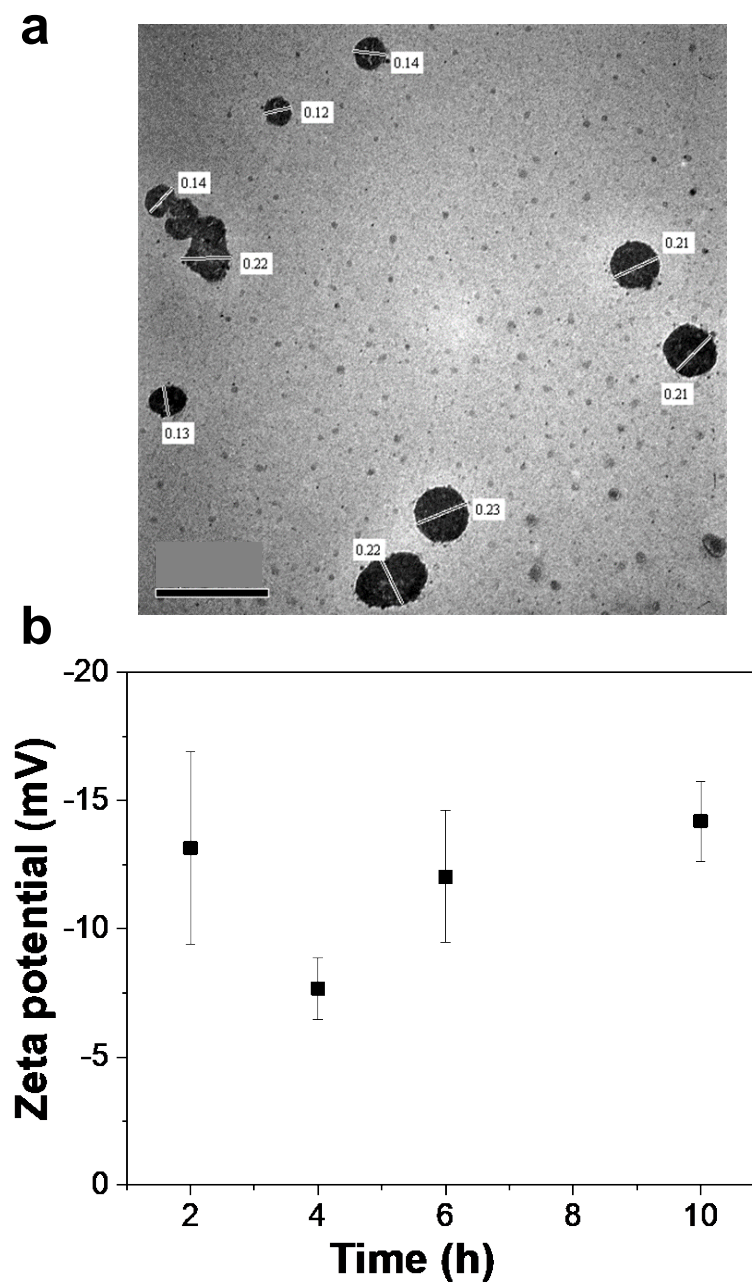


Figure S9. (a) TEM image and (b) zeta potential of the MnO_x particulates formed from the oxidation of Mn(II) by 5.0 mg/L Cl₂. Other experimental conditions: NaCl = 1.0 mM, Mn(II) = 100 µg/L, pH = 7.7 ± 0.1, open to air. The error bars are the standard deviations of triplicate measurements. The lines and numbers in (a) show the diameters of particles.

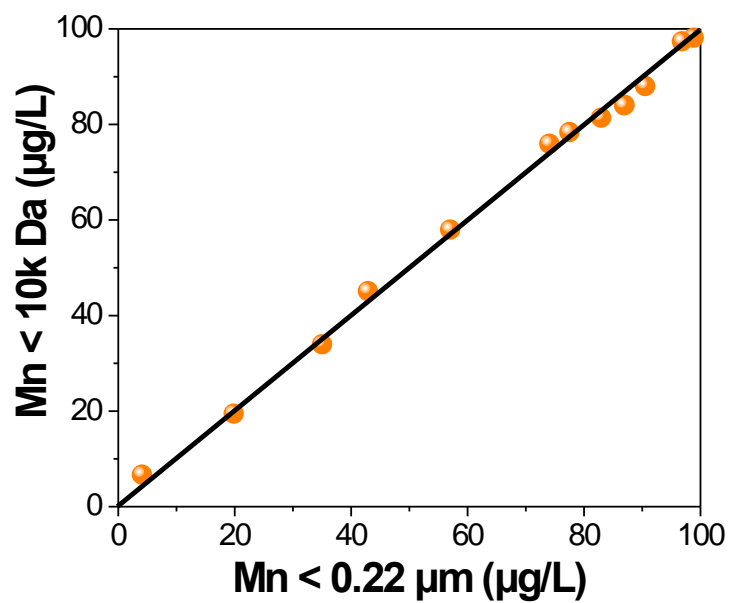


Figure S10. Comparison of Mn that passes through a 0.22 µm -filter and a 10k Da -filter in the Cu(II)-containing system. The solid line with a slope of 1 was drawn to indicate that the dissolved Mn(II) concentrations defined by the two kinds of filters were the same. Experimental conditions: NaCl = 1.0 mM, Mn(II) = 100 µg/L, Cu(II) = 100 µg/L, pH = 7.7 ± 0.1, open to air.

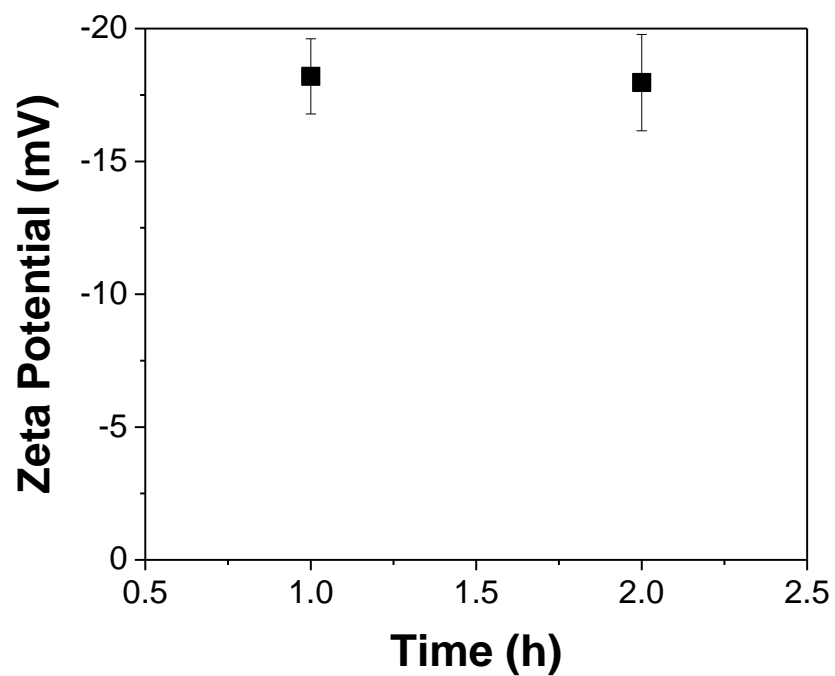


Figure S11. Zeta potential of Mn particles ($\text{MnO}_x\text{-Cu(II)}$) formed through Mn(II) oxidation in the system containing 100 $\mu\text{g/L}$ Cu(II). Other experimental conditions: NaCl = 1.0 mM, Mn(II) = 100 $\mu\text{g/L}$, pH = 7.7 ± 0.1 , Cl_2 = 1.0 mg/L, open to air. The error bars are the standard deviations of triplicate measurements.

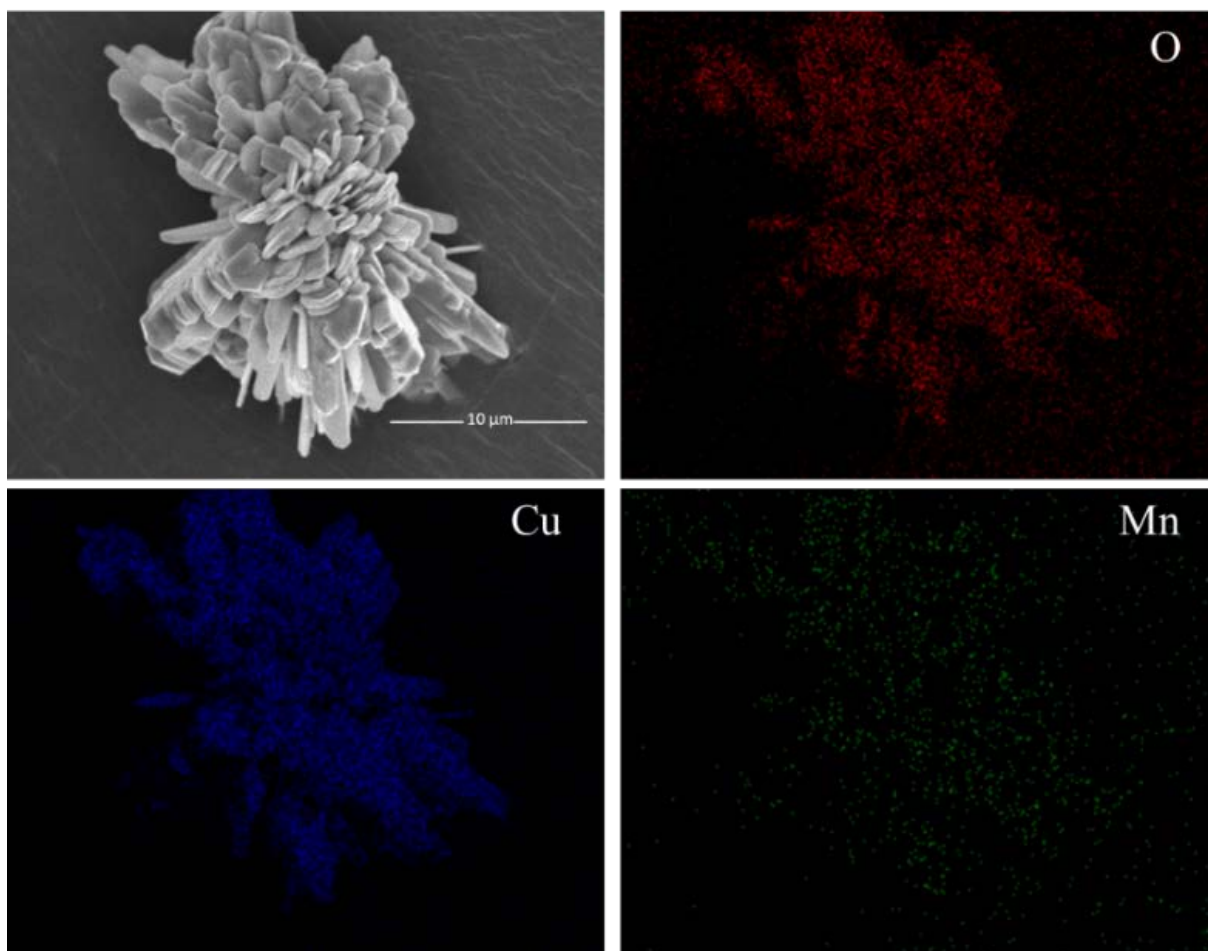


Figure S12. SEM image and EDS mapping of CuO particles collected after Mn(II) oxidation (reaction proceeded for 3 hours). Experimental conditions: NaCl = 1.0 mM, Cl₂ = 1.0 mg/L, CuO = 100 mg/L, Mn(II) = 100 μg/L, pH = 7.7 ± 0.1, open to air.

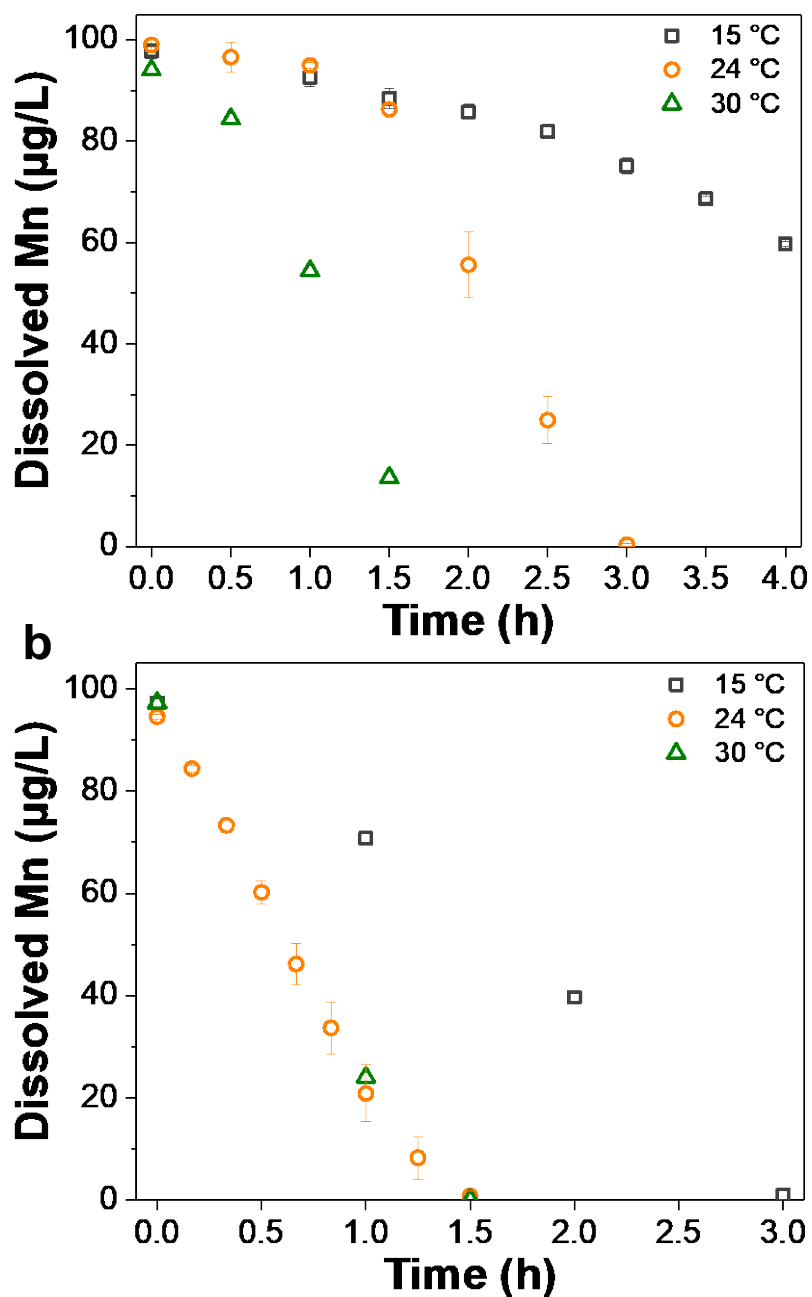


Figure S13. Effect of temperature on Mn(II) oxidation by chlorine in the presence of (a) 100 µg/L Cu(II) (added as CuSO₄) and (b) 100 mg/L CuO, respectively. Other experimental conditions: NaCl = 1.0 mM, Mn(II) = 100 µg/L, Cl₂ = 1.0 mg/L, pH = 7.7 ± 0.1, open to air. The error bars are the standard deviations of duplicate experiments.

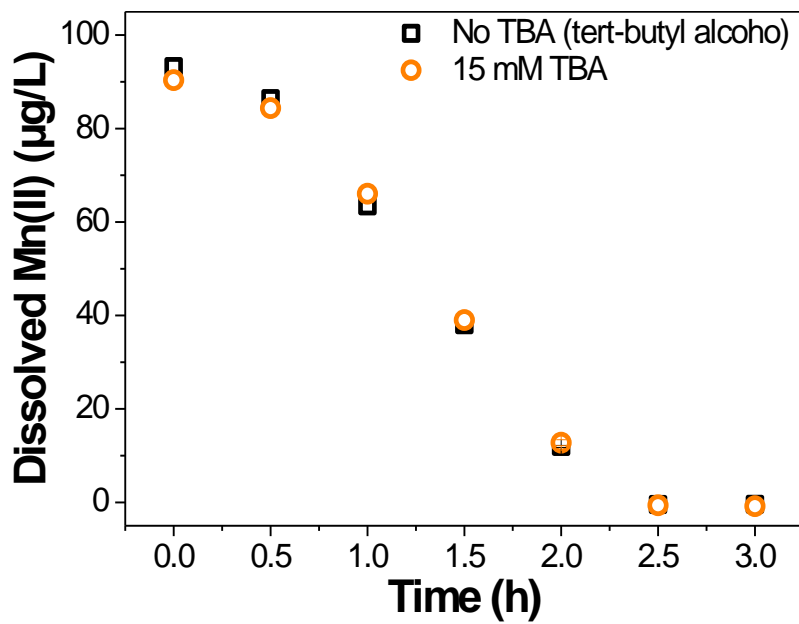


Figure S14. Effect of TBA on Mn(II) oxidation in the presence of $100\ \mu\text{g/L}$ Cu(II), $1.0\ \text{mg/L}$ Cl_2 at pH 7.7. Other conditions: NaCl = $1.0\ \text{mM}$, open to air.